NASA TECHNICAL NOTE

NASA TN D-1982

DYNAMIC RESPONSE OF HAMMERHEAD LAUNCH VEHICLES TO TRANSONIC BUFFETING

by Henry A. Cole, Jr.

Ames Research Center

Moffett Field, California

NATIONAL AERONAUTICS AND SPACE ADMINISTRATION • WASHINGTON, D.C. • OCTOBER 1963

TECHNICAL NOTE D-1982

DYNAMIC RESPONSE OF HAMMERHEAD LAUNCH VEHICLES TO TRANSONIC BUFFETING

By Henry A. Cole, Jr.

Ames Research Center
Moffett Field, California

NATIONAL AERONAUTICS AND SPACE ADMINISTRATION

NATIONAL AERONAUTICS AND SPACE ADMINISTRATION

TECHNICAL NOTE D-1982

DYNAMIC RESPONSE OF HAMMERHEAD LAUNCH VEHICLES TO TRANSONIC BUFFETING*

By Henry A. Cole, Jr.

SUMMARY

The static and dynamic buffeting characteristics of a particular launch vehicle with a payload diameter greater than the booster diameter are studied in detail through use of measurements on rigid, forced-oscillation, and free-oscillation models. The results are presented in the form of spectral densities and probability distributions. Dynamic transfer functions are used to show the amplification of buffeting loads due to unstable aerodynamic damping.

INTRODUCTION

Fluctuating pressures on rigid bodies due to transonic buffeting have been investigated for a large number of configurations at the Ames Research Center as reported in references 1 and 2. However, rational prediction of the loads on the full-scale flexible vehicle also requires a knowledge of the fluctuating pressures on a body in motion; consequently, a study of the dynamic response of flexible models was undertaken. The results from dynamic model tests have shown that certain nose shapes are unstable so that buffeting loads are amplified many times. The purpose of this paper is to present some of these results which show the relation of dynamic amplification to the dynamic response function.

DYNAMIC MODEL TECHNIQUE

In order to cover a wide range of configurations in a short time, the model was made as simple as possible. An examination of the bending modes of a typical booster rocket (fig. 1) showed that the nose portion of the modes is nearly a straight line. Since most of the input to the mode comes from this part of the mode, it was decided to approximate the first and second bending modes by a straight segment as shown. To obtain more accurate representation of the mode, an analytical method, such as reference 3, can be used to include the damping of the part of the mode behind the nose segment, or a complete dynamic model as reported in reference 4 can be used.

---

*This paper contains unclassified portions of a paper presented to the Seventh Symposium of Ballistic Missile and Space Technology, U. S. Air Force Academy, Colorado, 13-16 August 1962.

A schematic drawing of the dynamic model installation is shown in figure 2. Provision was made for two types of dynamic tests, forced oscillation with a hydraulic drive and free oscillation on a spring and damper. The bending moment output in either case is measured by strain gages.

Scaling

A number of difficulties arise in considering the proper scaling of the dynamic model so that it is representative of the full-scale vehicle. First of all, the Mach number and Reynolds number should be the same. The first of these conditions is easily met, but the second condition can only be approximated because model size is limited by blockage conditions of the wind tunnel. Secondly, to maintain geometric similarity of the flow, the reduced frequencies of model and full-scale vehicle should be the same. For example, if the full-scale vehicle has a first-bending frequency of 2.5 cps, then a 1/8-scale model must have a natural frequency of 20 cps. Unfortunately, most wind-tunnel sting supports have one or more natural frequencies in this range so the dynamics of the sting support must also be taken into account. It is advisable to put the model frequencies between the sting frequencies. Consequently, unless the sting support frequencies can be changed, the model frequencies available are limited. Thirdly, the motion amplitude of the model and full-scale vehicle should be the same.

Herein lies a real difficulty. The breaking amplitude of a launch booster in the first mode can occur with a nose slope of about $1/8^{\circ}$. Forced-oscillation tests at these amplitudes with models are extremely difficult because of accuracy requirements that arise from the low signal-to-noise ratio during tests in transonic flow.

After all of the above factors were considered, it was decided that the model should be built as light as possible to alleviate sting coupling problems and to obtain representative reduced frequencies with existing dynamic balance springs. To reach a frequency of 20 cps, the 3-foot models with a 7-inch-diameter base were built with a weight of about 5 pounds and a moment of inertia of 0.5 slug-ft^2. This was done by a sandwich construction of several layers of a 0.005-inch Fiberglas with a 2 lb/ft^3 Stafoam filler. A photograph of one of these models is shown in figure 3.

Initial free-oscillation tests were made on the hydraulic balance spring. In the course of these experiments, some difficulties were experienced with the damping of pinned joints. As a result, a free-oscillation support system was built as shown in figure 4. The main support is a simple cantilever spring instrumented with strain gages. A damper plate is mounted parallel to the main spring and connected through strain gages. Minimum damping ratio of the system is 0.017. An air brake activated by a limit switch serves as a safety device if the model diverges.

DYNAMIC RESPONSE TO BUFFETING OF MODEL WITH 30° NOSE, 10° BOATTAIL ANGLE

To demonstrate the effect of motion on loads due to buffeting, the model with a 30° nose and 10° boattail angle will be used as an example. As shown by the mathematical model in figure 5, the output bending moment, M_o, of the model in motion is related by a transfer function to the bending moment on the rigid model, M_i. The first second-order denominator term represents the model mode and each sting mode introduces a second-order numerator term and a second-order denominator term. In this section, the frequency response characteristics of this dynamic response function will be developed, and then will be used to relate measured power spectral density of bending moment on a rigid model to that measured on a model in free oscillation in accordance with the equation shown in figure 5.

Determination of Frequency Response

The frequency response of the dynamic model installation with wind off was measured by forced oscillations of the model with a hydraulic drive as indicated in figure 5. The results are given in figure 6 and the effects of the sting first and second bending modes are evident. The damping for this model is higher than the usual structural damping because the model had to be stabilized for unstable aerodynamic damping as will be shown later.

With wind on, the transfer function has to be corrected for aerodynamic forces and, for this purpose, the measured aerodynamic characteristics will now be presented.

Static derivative.- The unusual characteristics of such a nose are evident from the static aerodynamic pitching-moment coefficients shown in figure 7. The extreme nonlinearity of the pitching moment is typical of the dynamically unstable configurations. Note that this nose is actually statically stable up to an angle of attack of about 4°. Such a configuration would be attractive from a gust load and control standpoint since it would relieve the loads and stabilize the vehicle. When oscillations occur on the nonlinear parts of one of these curves, it is important to maintain the amplitudes in the model that are similar to those in the full-scale vehicle.

Damping derivative.- The aerodynamic damping derivative measured on this model is shown in figure 8 for several amplitudes of oscillation indicated by α_m. It may be seen that the model becomes dynamically unstable at a Mach number of about 0.8. The relationship of the aerodynamic damping derivative to damping ratio is given here for reference.

$$\zeta = \frac{-(C_{m_q} + C_{m_{\dot{\alpha}}})\rho V d^4}{32\, M l_n^2 f}$$

where

d base diameter, ft

f frequency, cps

l_n nose length, ft

M generalized mass of moving model, slugs

V velocity, ft/sec

ρ mass density of air, slugs/ft^3

It should be noted that if frequency is held constant, the damping ratio is inversely proportional to the generalized mass. In the case of a complete vehicle, the damping derivative for the part of the vehicle aft of the node line would have to be calculated and added to the part measured for the nose section, and the generalized mass for the complete mode would be used in the equation.

For the model, the effect of aerodynamic forces was calculated by including C_{m_α} and $C_{m_q} + C_{m_{\dot{\alpha}}}$ in the transfer function. The corrected peak is shown in figure 6 and it may be seen that the aerodynamic derivatives increased the frequency and raised the peak. This point then represents the peak amplification with wind on and will be used later to compare the measured power spectral densities of the rigid and free-oscillation models.

Measured Bending Moment on Rigid Model

The power spectral density of the measured fluctuations of bending moment on the rigid model is shown in figure 9. This spectrum was obtained from a time history of the direct electrical summation of outputs from 84 dynamic pressure transducers installed on the surface of the model. The transducers were at 19 longitudinal stations with 4 and 8 transducers per station, and were adjusted for sensitivity to account for the desired area-moment segment of the model represented by each transducer. In this case, the bending moment was obtained about the center of rotation of the free-oscillation model. The spectrum as shown has been corrected for a 20-percent difference in rigid and dynamic model sizes, and has also been smoothed to eliminate the scatter that appears on plots from a spectrum analyzer. The level shown is the mean level within the stylus swing.

Measured Bending Moment on the Free-Oscillation Model

The power spectral density of bending moment at the base of the free-oscillation model is shown in figure 10. This spectrum was calculated by applying Fourier analysis to a 30-second portion of the time history. It should be noted that the rms motion of 0.47° falls within the linear range of the aerodynamic derivatives so that the frequency response from figure 6 should be applicable. Also shown in the figure for comparison is Φ_i of the rigid model.

The large amplification of bending moment due to motion is apparent on the figure. The main purpose of this study was to determine whether the dynamic amplification could be predicted by the dynamic response function in accordance with the equation

$$\Phi_o = |TF|^2 \Phi_i$$

As seen in the figure, the amplification is predicted very well when the aerodynamic damping derivative is included in the TF as shown in figure 6. However, when the damping derivative was neglected, the peak was underestimated considerably.

Prediction of Peak Values of Bending Moment

As pointed out in reference 5, the power spectrum by itself is not of much use to the structural designer, because he is interested in absolute values. Consequently, we turn now to a study of the time history of motion. A shadowgraph of the flow is shown in figure 11 to give a visual picture of the process. During free oscillations, the short shock wave appearing in the turbulent region was observed to undergo considerable motion; thus, it is indicated that the flow separation may be within the turbulent region.

A sample of the time history of motion is shown at the top of figure 12. It may be seen that the motion consisted of random bursts of oscillation near the natural frequency. From 3000 points measured over a 30-second interval, the probability of exceeding the rms by various amounts was calculated as shown by the circles. Also shown in the figure is the theoretical curve for a normal distribution and it may be seen that the agreement is quite good. A study of the peak values in the 30-second interval is shown in figure 13. Also shown in the figure is the theoretical curve for a Rayleigh distribution and once again the agreement is quite good. The observation on peak values is in accordance with reference 6 which shows that the envelope of the peaks of a random process when passed through a narrow band-pass filter will follow this distribution. Consequently, these results show that the peak values may be predicted from the rms for the case in which one mode is dominant.

CONCLUDING REMARKS

On the basis of partial mode dynamic model tests, it has been shown that a certain hammerhead nose shape is unstable aerodynamically and that the loads due to buffeting may be magnified many times. The studies of power spectrum and probability distributions indicate that fairly good predictions of the loads may be made by multiplying the power spectrum of rigid body moments by the square of the absolute value of the dynamic transfer function with aerodynamic derivatives included. Furthermore, it appears that the peak bending moment may be estimated on the basis of a Rayleigh distribution for the case of one dominant

mode. However, in the prediction of dynamic loads due to buffeting, it should be remembered that the uncertainties involved in the damping measurements can cause large errors in the prediction.

Ames Research Center
National Aeronautics and Space Administration
Moffett Field, Calif., July 8, 1963

REFERENCES

1. Coe, C. F.: Steady and Fluctuating Pressures at Transonic Speeds on Two Space-Vehicle Payload Shapes. NASA TM X-503, 1961.

2. Coe, C. F.: The Effects of Some Variations in Launch-Vehicle Nose Shape on Steady and Fluctuating Pressures at Transonic Speeds. NASA TM X-646, 1962.

3. Bond, R., and Packard, B. B.: Unsteady Aerodynamic Forces on a Slender Body of Revolution in Supersonic Flow. NASA TN D-859, 1961.

4. Runyan, H. L., Jr., and Rainey, G. A.: Launch-Vehicle Dynamics. NASA TM X-607, 1961.

5. Getline, G. L.: Structural Response to Random and Discrete Noise Inputs. AIA Symposium Proceedings on Structural Dynamics of High Speed Flight, vol. 1, 1961.

6. Rice, S. O.: Mathematical Analysis of Random Noise, Selected Papers on Noise and Stochastic Processes, Dover Pub., N. Y., 1954.

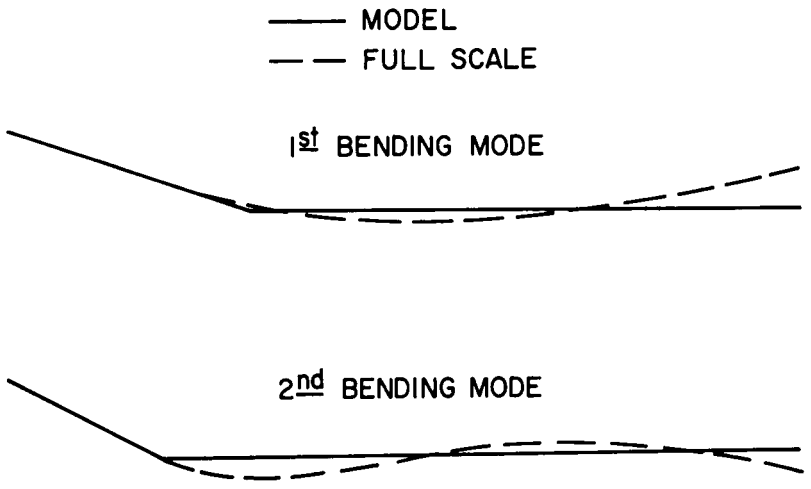

Figure 1.- Approximation of bending modes.

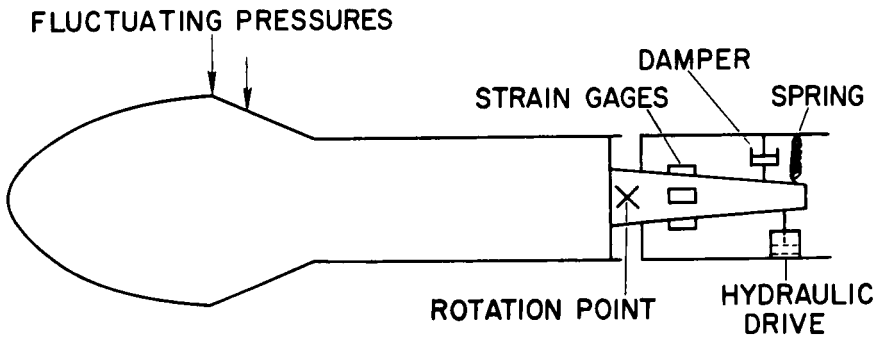

Figure 2.- Schematic drawing of dynamic model installation.

A-28133

Figure 3.- Photograph of model in Ames 14-Foot Transonic Wind Tunnel.

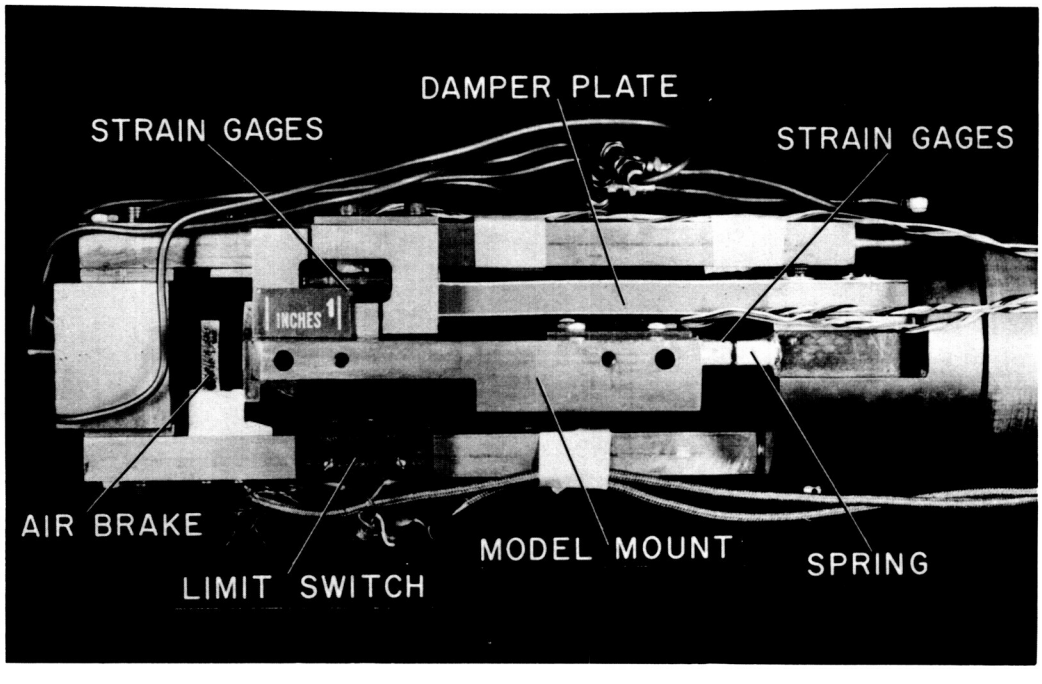

A-29040.2

Figure 4.- Photograph of spring and damper installation.

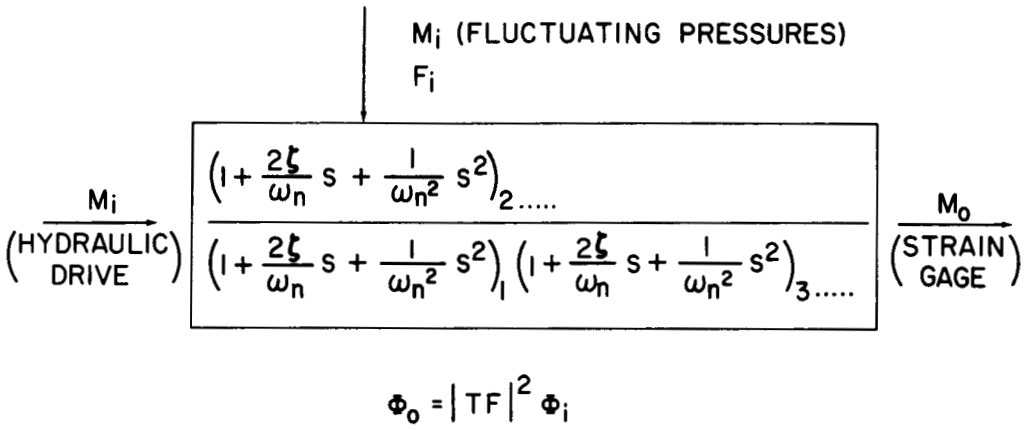

Figure 5.- Mathematical model of dynamic model installation.

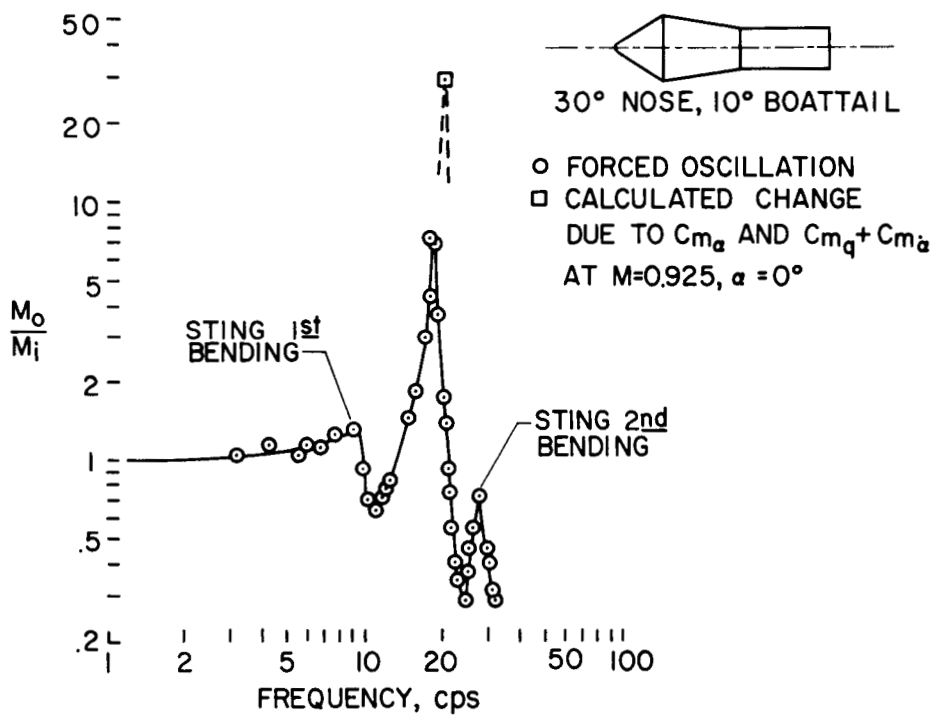

Figure 6.- Measured frequency response of model on spring and damper.

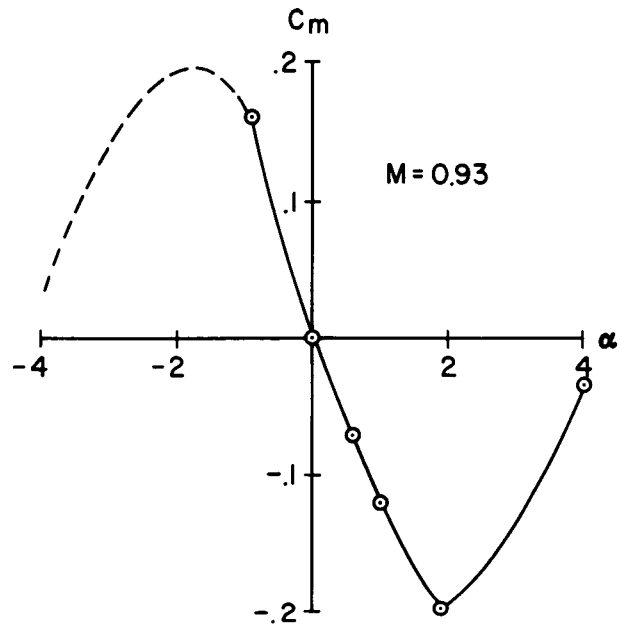

Figure 7.- Variation of moment coefficient with angle of attack for model with a 30° nose and 10° boattail angle.

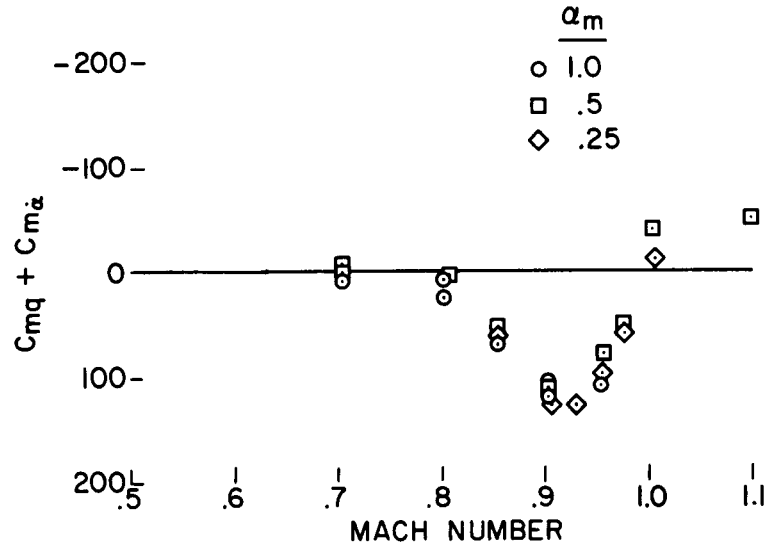

Figure 8.- Damping measurements for model with a 30° nose and 10° boattail angle at 0° angle of attack.

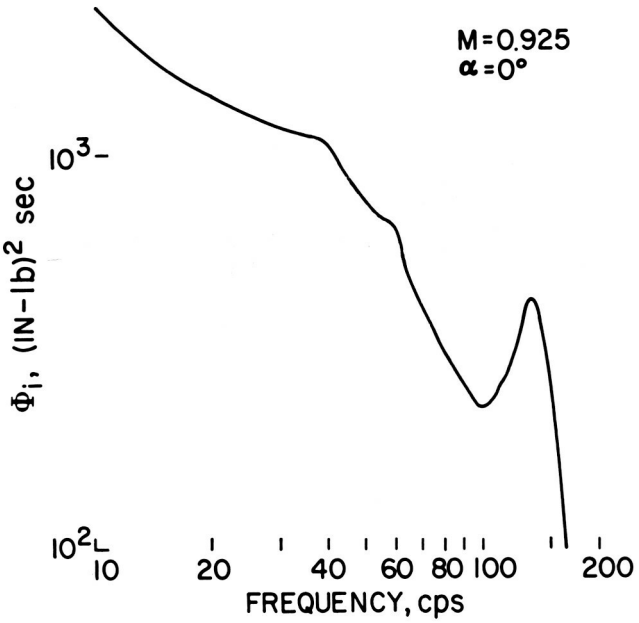

Figure 9.- Measured power spectral density of bending moment on rigid model with a 30° nose and 10° boattail angle.

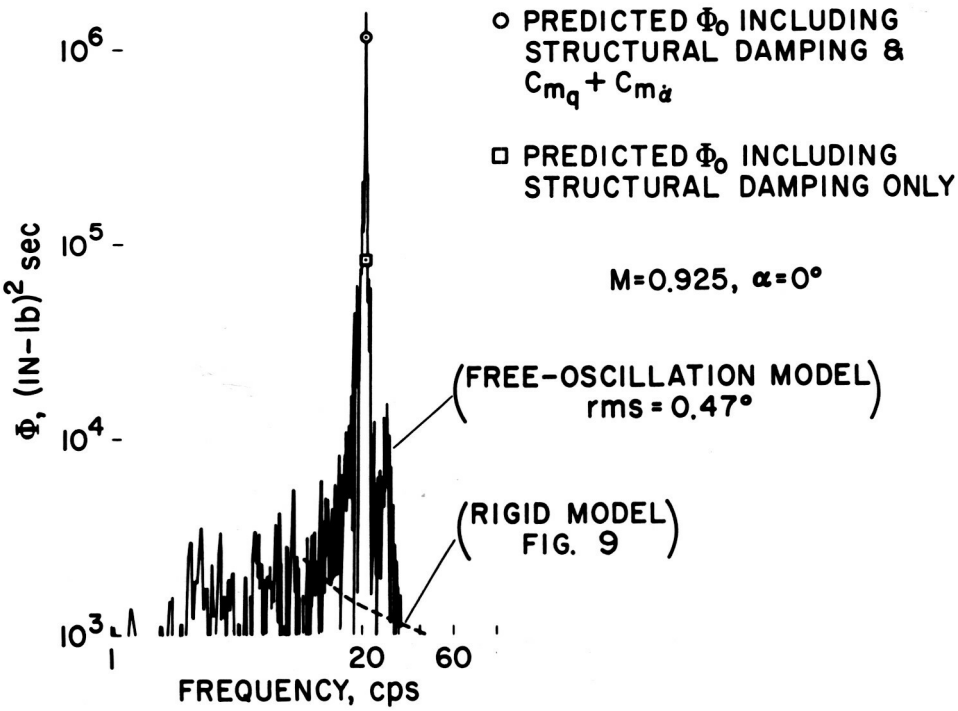

Figure 10.- Measured and predicted power spectral densities for model with a 30° nose and 10° boattail angle.

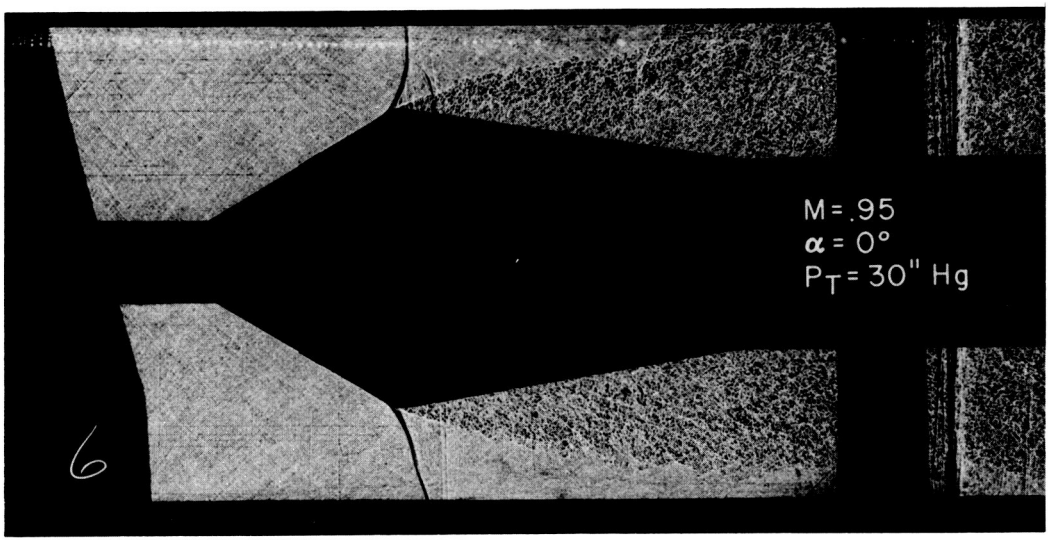

A-31111

Figure 11.- Shadowgraph of model with 30° nose and 10° boattail angle at a Mach number of 0.95.

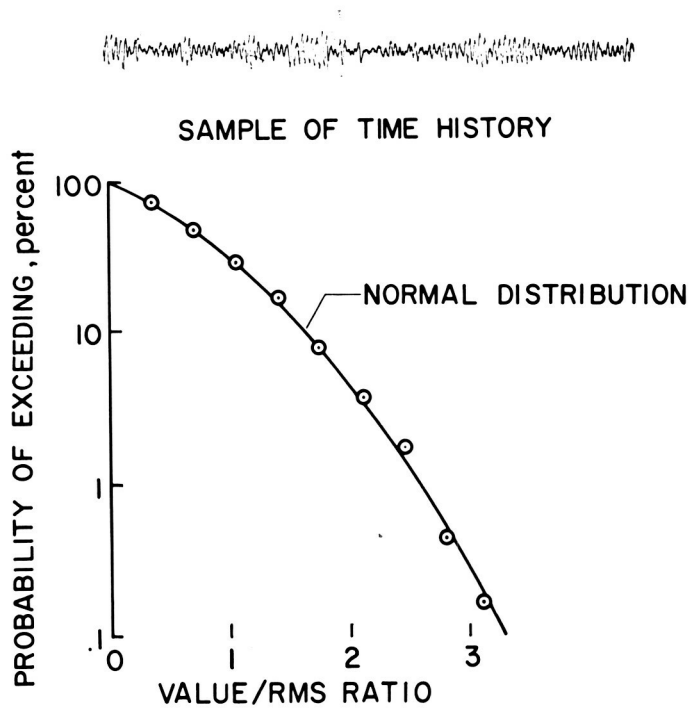

Figure 12.- Comparison of distribution of 3000 values with normal distribution (rms = 788 in.-lb).

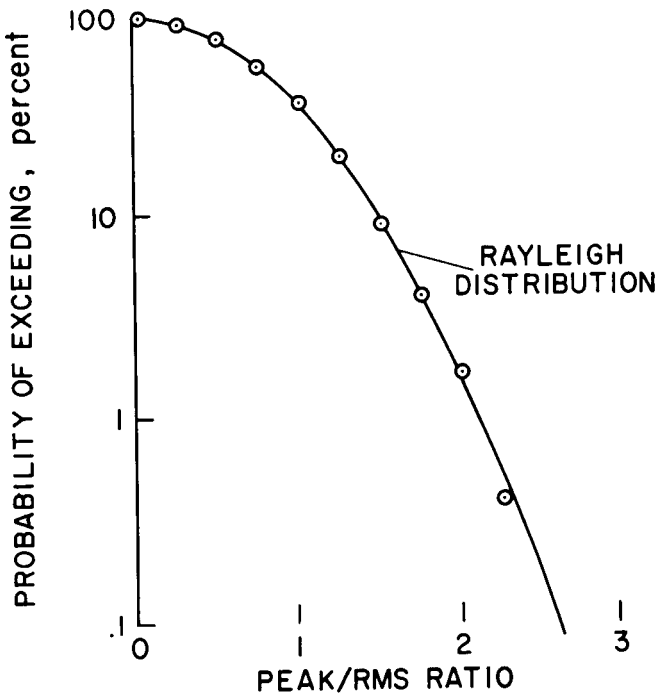

Figure 13.- Comparison of distribution of 1230 peak values with Rayleigh distribution (rms = 1188 in.-lb).